Synthesis and Luminescence of Lanthanide Ions in Nanoscale Insulating Hosts

Brian M. Tissue*

Department of Chemistry, Virginia Polytechnic Institute and State University Blacksburg, Virginia 24061-0212

Received April 1, 1998. Revised Manuscript Received June 24, 1998

This review summarizes recent work in nanostructured insulating materials that contain optically active lanthanide ions. These materials find applications in lasers, optical amplifiers, and optical-display phosphors. This review concentrates on the synthesis and luminescence spectroscopy of lanthanide-containing nanostructured particles, films, and composites. Spectroscopic studies range from basic luminescence spectroscopy and quantum efficiency measurements to high-resolution spectroscopic studies that investigate the phonon dynamics and electron−phonon interaction as a function of particle size. This review identifies several areas for further study, including the location, distribution, or segregation of dopants in nanoparticles; the efficiency of energy transfer across interfaces; and the effects of quantum confinement or changes in phonon dynamics and electron−phonon interactions on the radiative and nonradiative relaxation rates in localized luminescent dopants.

Contents

I. Introduction

A. Scope of the Review. Lanthanide (also known as rare-earth) ions in insulating hosts find uses in a wide variety of applications,[1−3] including phosphors for fluorescent lighting, display monitors, and X-ray imaging;[4−6] scintillators;[7] lasers;[8] and amplifiers for fiber-optic communication.[9] The luminescence efficiency of these materials is often limited by the dynamics of the lanthanide ion, which depends on interactions with the insulating host. The rationale to study nanostructures of lanthanide-doped insulating materials arises because the spectral and dynamic properties of these technologically important materials change when the reduced dimensions affect the chemistry and physical properties of the host. In a similar manner, the lanthanide dopant can serve as a sensitive probe of the chemistry and structure of its host. This review includes investigations of how the particle dimensions, composition, processing, and morphology of a host affect the optical properties of a lanthanide dopant.

Nanocrystalline and nanostructured materials are typically defined as polycrystalline solids with particle diameters or grain sizes of 100 nm or less. Nanocrystals can form in new phases[10] and exhibit enhanced structural, electronic, or optical properties.[11−15] This review describes recent advances in the synthesis and characterization of nanostructured insulators that contain optically active lanthanide ions. These materials take advantage of size-induced changes to create new or enhanced materials for advanced phosphor and photonic applications. Some potential optical applications include lasers,[16] solar-energy converters,[17] optical amplifiers,[9] and photo- or cathodo-excited optical phosphors.[18−21] To maintain a concise and focused review, this paper does not review advances in nanocrystalline semiconductors, which are being studied extensively for their unique size-dependent quantum-confinement effects,[22−25] nor does it include the active research in lanthanide-doped fullerenes[26,27] or porous silicon.[28,29] After some general considerations, this review is organized into sections on nanoparticles, nanostructured films and composites, and dynamic and high-resolution spectroscopic methods. This organization is somewhat arbitrary, but it groups many related topics together for convenience.

B. Background. The development of new synthesis and processing methods creates opportunities to prepare particles, films, and composites with nanometer dimensions. Preparing nanoscale host materials can change the physical properties of the host, which affects the luminescence and dynamics of an optically active dopant. Investigating and understanding these materials will be important for optimizing their emissive properties for technological applications in future communication and display devices. Several groups have reported particle-size-dependent phenomena in lanthanide-doped nanoparticles that affect emission lifetime,[30,31] luminescence quantum efficiency,[19,31] and concentration quenching.[32] Some effects have been attributed to quantum-confinement effects when the particle diam-

* E-mail address for correspondence: tissue@vt.edu

10.1021/cm9802245 CCC: $15.00
Published on Web 09/16/1998

eter is less than 5 nm.[31] In both Tb^{3+}:ZnS and Mn^{2+}:ZnS, the luminescence lifetime becomes shorter by several orders of magnitude.[31,33] These size-dependent effects are postulated to result from mixing of the s−p electrons of the host with the d−f valence electrons of the activator due to quantum confinement, causing the normally forbidden d−d or f−f transitions to become allowed.[31]

Theoretical predictions suggest that the phonon density-of-states and the electron−phonon interactions are strongly modified in nanometer-sized particles.[34] The strength of the electron−phonon interaction appears to grow inversely with the square of particle diameter ($\sim 1/d^2$) in semiconducting nanoparticles,[35,36] and a recent calculation of phonon satellites in the photoluminescence of CdS nanocrystals indicates an enhanced phonon-assisted transition probability.[37] Although research in nanostructured semiconductors is beginning to produce a clear theoretical picture of these materials, very little theoretical work has addressed the size-dependence of localized emissive ions in nanostructured hosts. What is clear is that the current theories and experimental database are inadequate to understand the optical properties of localized luminescent centers in nanostructures.

Reducing the particle size could be deleterious if the close proximity of lanthanide ions to a higher relative concentration of surface defects increases the quenching of optical emission.[5] Although many technologically important materials contain dopants, very little work has addressed dopant distribution or defect chemistry in nanocrystalline materials. In fact, the concept of dopant (or defect) distribution and segregation becomes ambiguous in particles in which a large fraction of the constituent atoms reside at or near a surface. The large surface-to-volume ratio is expected to affect the dopant and defect distribution between the interior, surface, and exterior (secondary phases) of the particles. Understanding the distribution of dopants and defects, i.e., the chemistry, in nanocrystalline materials will be crucial for understanding their bulk properties. The presence of surface defects is a major factor affecting the efficiency of nanocrystalline phosphors,[38] and the efficiency of conventional phosphors decreases with decreasing particle size due to quenching by surface defects.[5] The ability to control these defects could lead to energy-efficient phosphor materials for the next generation of projection and flat-panel displays.

Preparing optically active nanostructures has the potential for discovering and investigating materials that exhibit unexpected and unique optical phenomena, such as possible enhanced coupling of the localized centers to electromagnetic radiation[31] or other confinement effects.[30] Preparing lanthanide-doped nanostructures also provides a new method to develop and study transparent composite materials. The reduced optical scattering of nanometer-sized particles allows the preparation and use of nanocrystals embedded in an amorphous matrix in applications such as lasers and amplifiers, which usually require high-quality crystals or glasses.[9] Using nanostructured composites in optical applications could simplify material preparation or allow the use of new host materials for which good crystals cannot be grown.

Another promising application for nanostructured materials is as phosphors for field-emission displays (FEDs).[39] These flat-panel displays use a cold-cathode (<1 keV) electron emitter tip to excite the phosphor screen. Unlike conventional phosphor particles, luminescent nanostructured materials are attractive for FED applications because their small size allows complete penetration by the low-voltage electrons for efficient material utilization. The close proximity of the phosphor particles to the emitter tips requires that the phosphor not outgas or sputter material that will poison the tips, so oxide materials are preferred compared to sulfides.

From a more fundamental standpoint, nanostructured materials can provide model systems to study surfaces. It is not possible to study the luminescence of dopant ions located at the surface of micron-sized particles because the large signal from ions in the interior of the particles obscures any signal from ions at the surface. The high surface-to-volume ratio of nanocrystalline particles results in a significant fraction of all atoms in the particle being at or near a surface, approximately 30−50% as particle diameters approach a few nanometers. Doping lanthanide ions in nanocrystals of these dimensions places a sensitive probe at the particle surface. This probe will be sensitive to any changes in surface crystallinity or reactions.

II. General Synthesis, Processing, and Characterization Considerations

A. Synthesis. There are a large number of methods for forming discrete metal oxide nanoparticles, including oxidation of metal nanoparticles,[40] vaporization/condensation of ceramics,[41] laser ablation,[42] laser-driven reactions,[43] flame and plasma processing,[44,45] solution-phase synthesis,[46−49] sol−gel processing,[50−52] electrospray and spray pyrolysis,[53−55] combustion synthesis,[56] high-energy mechanical milling,[57] and self-assembly.[58,59] Many of these particle synthesis methods can be modified to create nanostructured films and nanocomposites. The surfaces of nanoparticles can be changed by chemical reactions or by dispersing the particles in a polymer or glass matrix. There are also a variety of synthesis and processing methods to prepare metal oxide nanocrystals in matrixes. The simplest embedding method is to disperse nanocrystals in solution and puddle cast in a polymer matrix.[9] The method to prepare samples for TEM analysis shows that nanocrystals dispersed in organic solvents by ultrasound for only short times remain in an open, although networked agglomerate.[60] It is also possible to modify the surfaces of nanocrystals to more intimately disperse them during a polymerization reaction[61] and to use self-assembly methods.[58] Surface modification methods present the possibility to embed nanocrystals in a variety of matrixes to adjust the phonon properties of the composites.[62] Optically active molecules have also been attached to semiconductor nanoparticles,[46,63] but not to insulators containing luminescent dopants.

Preparing and studying nanocomposites will more closely mimic the environment of nanocrystals in actual devices and can provide protection from environmental degradation. The high surface area of nanocrystals produces a high reactivity and results in an accelerated

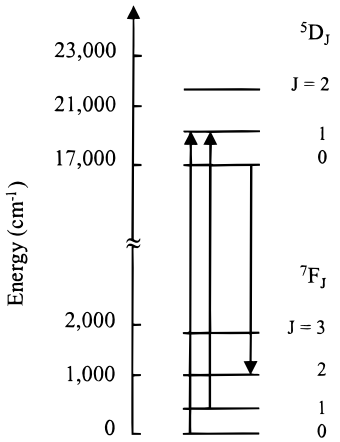

Figure 1. Partial energy-level diagram of the Eu^{3+} ion in solids. Each level can be split into $2J + 1$ sublevels. Two upward arrows show absorption transitions, including a hot-band transition originating from the $^7F_1$ level, and the downward arrow shows the strong red luminescent $^5D_0 \rightarrow {}^7F_2$ transition.

rate of reaction with atmospheric water and CO_2 compared to micron-sized particles. We observe a decrease in the luminescence intensity of gas-phase-condensed Eu^{3+}:Y_2O_3 nanocrystals within 6 months of preparation when stored in a regular lab desiccator. This decrease in intensity of the nanocrystal luminescence over time is attributed to formation of an amorphous hydroxide phase.

B. Physical Characterization. Nanocrystals and nanostructured films for luminescent applications are routinely characterized by powder X-ray diffraction (XRD), transmission−electron microscopy (TEM), and scanning-electron microscopy (SEM). Less common but not less powerful characterization methods include reflectance Fourier transform infrared (FTIR), absorption spectroscopy, extended X-ray absorption spectroscopy (EXAFS), atomic force microscopy (AFM), light scattering, and BET surface area measurements. AFM is being used more frequently, although preparing atomically thin AFM tips to image particles of less than 10-nm diameter can be very difficult. The advantage of the AFM is that it provides the capability to study the morphology of as-prepared nanoparticles and nanocomposites, unlike TEM, which usually requires dispersion of the particles to avoid a thick film of sample. These diffraction and imaging characterization tools will determine the crystal phase, average particle or grain diameter, particle-size distribution, and the morphology of the samples. The X-ray diffraction line widths and TEM and AFM images can provide independent measures of the particle size. Luminescence spectra or quantum-efficiency measurements excited by optical photons, electrons, or X-rays can be made with lab-scale spectrometers.

C. Site-Selective Optical Spectroscopy. The lanthanide emitters, which are so important in technical applications, also serve as sensitive probes of their local environment. In the lanthanides, the outer 5s and 5p electrons shield the 4f electrons from gross perturbations with the lattice, so the 4f orbitals retain their hydrogenic character.[64] Therefore, the position of the energy-level multiplets do not vary significantly from host to host (see Figure 1) and the intraconfigurational transitions between the 4f levels are sharp (on the order of 10^{-3} cm^{-1}, full-width at half-maximum). The 4f orbitals are sensitive to the local crystal field, which splits the *J*-multiplet energy levels on the order of hundreds of wavenumbers. The splitting pattern depends on the strength of the crystal field and the local site symmetry. The optical spectra therefore consist of sharp lines that are characteristic of the local environment and serve as sensitive microprobes of the crystallographic site(s) the lanthanide ion occupies in the solid host. The luminescence dynamics depend on ion-lattice (electron−phonon) and ion−ion interactions and on the phonon spectrum of the host. Clustering of the lanthanide dopant changes the degree of ion−ion interactions and the luminescence dynamics serves as a diagnostic to study the defect chemistry in a material.[65]

Optical spectroscopy of lanthanide ions can therefore contribute to the understanding of the structure, phase distribution, crystallinity, phonon spectrum, electron−phonon interactions, and defect chemistry in nanostructured materials. Such measurements have been demonstrated in a wide variety of bulk materials. Luminescence measurements are sensitive enough to detect a small number of emitting ions, as demonstrated by photoluminescence studies of thin films,[66] and they can be performed in any geometry, allowing spectroscopy of opaque samples.[67] Site-selective laser spectroscopy of dopant ions in crystals and glasses has been used to study defect equilibrium,[65] defect aggregation kinetics,[68] precipitation,[69] phase transformations,[70] and the degree of disorder or crystallinity.[71] Site-selective spectroscopy can also be used to monitor the effects of materials processing such as thermal annealing, laser treatment, and plasma etching. In some cases, it is possible to use lanthanide spectroscopy in situ to monitor a material as it is being treated.

Sample are often cooled to low temperature (<77 K) to enhance the sensitivity and resolution in the spectra. A narrow line width laser can be tuned selectively to an individual feature in an absorption spectrum to obtain high-resolution fluorescence spectra and time-resolved fluorescence transients of each distinct lanthanide environment. Absorption lines that produce the same fluorescence spectrum and fluorescence lifetimes are assigned to the same ion site. In this way all of the lines in an absorption spectrum can be assigned to elucidate the impurity distribution. The number of spectral lines and splitting pattern, the lifetime, and observations of fast nonradiative relaxation or energy transfer give clues to the local nature of each site. Similarly, disordered systems can be characterized by recording fluorescence-line-narrowed spectra as the laser is tuned across the distribution of different sites.

The restricted geometry of ions in nanoparticles is expected to affect the luminescence decay compared to energy transfer and electron−phonon interactions in a bulk crystal. Many of the models of energy transfer average a distribution of distances between donor and acceptor sites that is not valid in nanoscale systems. The observation of single-exponential decay in the excited-state luminescence decay in 4-nm Eu_2O_3 supports this hypothesis.[30] Donor−acceptor transfer in molecular-beam epitaxy (MBE) grown films has also been observed to be modified due to restricted geometry

and to become less effective in the 2D geometry.[72] Energy transfer through space has been used to measure distances as long as approximately 8 nm in molecular systems.[73] Studying energy transfer between lanthanides in different host particle with dimensions of less than 10 nm will no doubt require a different theory than for bulk materials.

III. Nanoparticles

An optical spectroscopic investigation of high surface area Eu_2O_3 (≤ 100-nm diameter) did not show significant line shifts due to the reduced particle size.[74] However, the lowest temperature available for recording spectra was 93 K, and thermal broadening might have obscured detection of any small changes in the inhomogeneous broadening or the peak positions. This catalytically active material was prepared by thermal dehydration of $Eu(OH)_3$, which produced cubic-phase Eu_2O_3. Cubic Eu_2O_3 (and cubic Y_2O_3) has two distinct crystallographic sites, one with C_2 and the other with S_6 local symmetry, which give rise to two sets of Eu^{3+} spectra.[75] Sheng et al. reported a change in the relative intensity of the luminescence from these two sites when the powders were exposed to water.[74] The relatively strong emission from Eu^{3+} ions in the C_2 site did not change, but the relatively weak emission from the other site decreased. The authors credit the change to preferential chemical attack of water on the S_6 cation site. Observing this change would be unexpected for large particle sizes due to the large luminescence signal from ions in the interior of the particles that obscure changes at the surfaces. This result indicates that luminescent probe ions could be useful to study the details of surface reactions if the surface-to-volume ratio is high. The transitions of the S_6 are weak because this site has inversion symmetry. The observed relative change might be enhanced if the distorted S_6 sites at the surfaces of the particle contribute disproportionately to the observed weak emission. This explanation could be verified by measuring the ratio of S_6 to C_2 luminescence as a function of particle size in cubic Eu_2O_3.

Cubic-phase Eu^{3+}:Y_2O_3 phosphors have been prepared by homogeneous precipitation by heating solutions of urea and metal nitrates at 80 °C.[76] The particle size could be controlled by stopping the reaction after different reaction times and ranged from 43 to 71 nm for reaction times of 1−2.5 h (after an initial 3 h heating). The strongest peak in the emission spectra ($^5D_0 \rightarrow {}^7F_2$) of these particles shifted from 614 to 610 nm as the particle size decreased from 71 to 43 nm. The peak wavelength for micron-sized particles was 618 nm. This shift in peak wavelength was attributed to a change in the crystalline field. Powder XRD showed that the lattice parameter of the nanocrystalline particles decreased from 1.200 to 1.1142 nm. This result suggests that the wavelength of laser or amplifiers based on nanostructured materials might be selectable over narrow spectral ranges for different physical sizes of the particles.

Cubic-phase Eu^{3+}:Y_2O_3 has also been prepared by combustion synthesis.[32,56,77,78] In this method metal nitrates (the oxidizer) react explosively with an organic fuel such as glycine. The reactants are mixed in an aqueous precursor solution and the reaction is initiated by evaporating the water in a furnace. The rapidity of the reaction results in particles with nanoscale diameters, which can be controlled by adjusting the fuel-to-oxidizer ratio. A major advantage of this procedure is that it can rapidly produce gram quantities of nanocrystalline material. The phosphor brightness can be maximized by optimizing the preparation conditions such as fuel-to-oxidizer ratio and furnace temperature. Annealing the as-prepared powders can also improve brightness by eliminating any residual nitrate or carbon. Ye et al. report changes in the charge-transfer excitation spectrum as a function of particle size that are attributed to surface effects.[32] For 70-nm diameter particles, they also report that the Eu^{3+} concentration can reach 14% before the onset of concentration quenching, which is double the onset concentration of 6−8% for conventional phosphor material.[75,77] This difference is attributed to a reduced energy-transfer rate due to the interfaces, so less energy can migrate to quenching sites. The change in concentration quenching also suggests that the close proximity of the surface does not introduce a large number of quenching surface defects.

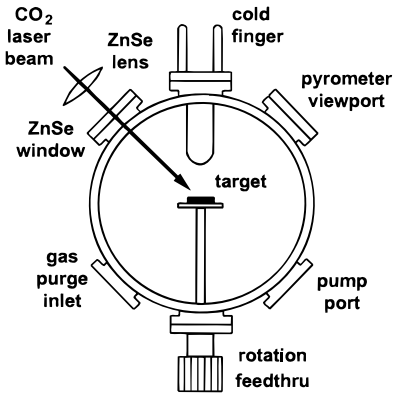

Figure 2. Schematic of a nanocrystal preparation chamber that uses CO_2-laser heating of a ceramic target.

Table 1. Effect of Chamber Pressure on the Resulting Size of Eu_2O_3 Nanocrystals

chamber pressure, Torr	average particle diameter, nm	crystal structure
400	18	monoclinic
100	12	monoclinic
10	6	transitional
1	4	cubic (disordered)

My group has refined a CO_2-laser-heated gas-phase condensation method to reproducibly prepare $Eu_xY_{2-x}O_3$ and other nanocrystals.[60] A CO_2 laser heats a ceramic target to vaporize material that forms gas-phase clusters, which collect on a coldfinger as nanoparticles with a narrow size distribution (see Figure 2). This procedure, which directly heats metal oxide starting material, produces nanocrystals under well-controlled conditions without needing a subsequent oxidation step. The disadvantage of the laser-heated process compared to solution, combustion, or spray-type synthesis methods is that it is not easy to scale-up to produce gram quantities of material.

The size of the resulting nanocrystals can be controlled by varying the chamber pressure, as illustrated in Table 1 for Eu_2O_3. Nanoparticles of Y_2O_3 show the same trend but are approximately 25% larger for the same conditions. Figure 3 shows an electron micrograph of 0.1% Eu^{3+}:Y_2O_3 prepared with 100 Torr of N_2

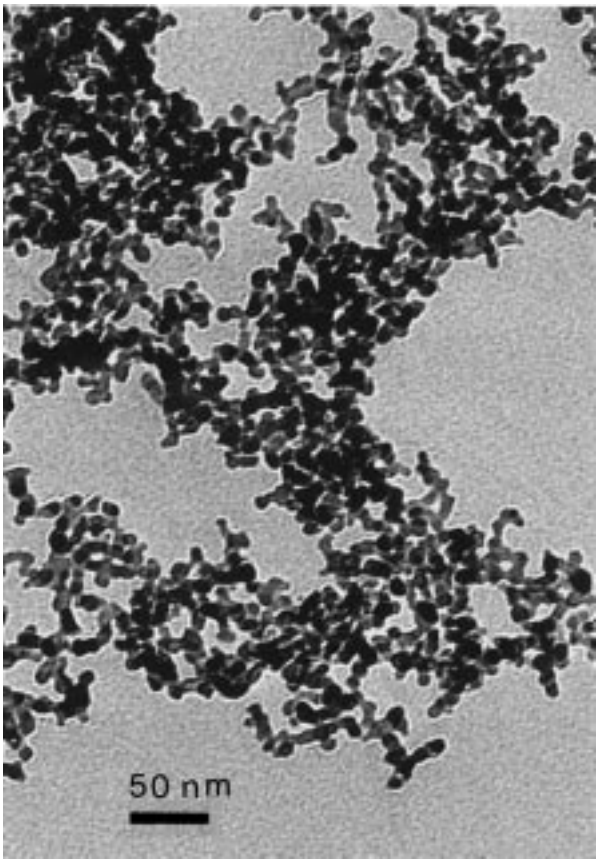

Figure 3. Transmission electron micrograph of 0.1% Eu^{3+}:Y_2O_3 prepared by CO_2-laser-heated gas-phase condensation at a chamber pressure of 100 Torr. The average particle size was 13 nm and the range of diameters was 5−21 nm. The magnification is 208 333.

in the preparation chamber. The open network of particles is very typical for gas-phase-condensed nanoparticles. Table 1 also indicates that for samples prepared by gas-phase condensation with average diameters from 10 to >20 nm, the majority of the sample forms in a high-temperature monoclinic phase. This phase is produced in other high-temperature methods for preparing nanoscale Y_2O_3.[40,45] Skandan et al. attributed the formation of nanocrystalline Y_2O_3 in the denser monoclinic phase under ambient conditions to an additional hydrostatic pressure component, resulting from the Gibbs−Thomson effect.[40] Although the lines are very broad, XRD patterns suggest that particles of less than approximately 6−7 nm form in the cubic phase. Preliminary annealing studies of 5-nm Y_2O_3 samples at temperatures as low as 150 °C show the broad XRD lines sharpening into the usual cubic-phase XRD pattern. The 6-nm sample labeled as having a transitional structure in Table 1 has an XRD pattern that is intermediate between the crystalline monoclinic pattern of larger particles and the very broad peaks in the 4-nm sample.

The Eu^{3+} solubility of as-prepared Eu^{3+}:Y_2O_3 nanocrystals (approximately 20-nm average diameter) is different from that of bulk cubic-phase material, which can contain >5% Eu^{3+}.[79] Nanocrystals prepared from 0.1% Eu^{3+}:Y_2O_3 starting material were single phase, but samples prepared from ≥0.7% Eu^{3+}:Y_2O_3 formed with a secondary Eu_2O_3 phase. To my knowledge, synthesis of Eu^{3+}:Y_2O_3 nanocrystals by solution or combustion

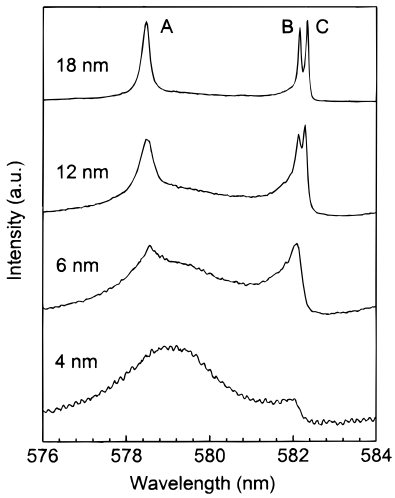

Figure 4. $^7F_0 \rightarrow {}^5D_0$ excitation spectra of nanocrystalline Eu_2O_3 at approximately 12 K. The spectra were recorded with a low-resolution monochromator at 624 nm and a boxcar gate width of 150 μs. The *y*-axis for all spectra in this paper is luminescence intensity in arbitrary units.

methods does not result in phase separation. The apparent solubility limit in gas-phase-condensed nanoparticles is attributed to a kinetic effect in the condensation. A side benefit of this phase separation is that it provides a simple means of preparing Eu_2O_3/Eu^{3+}:Y_2O_3 nanocomposites of two spectrally distinct phases.

The $^7F_0 \rightarrow {}^5D_0$ excitation spectra of Eu_2O_3 nanocrystals in Figure 4 show the typical broadening and line shifts that occur as the particle size decreases.[80] This same trend is also observed for other excitation transitions and in the luminescence spectra.[30] The three strongest lines in the excitation spectrum of the 18-nm particles arise from the three crystallographic lattice sites in the monoclinic phase. The relatively broad line at 579 nm is visible in the 18-nm sample when the *y* scale is expanded, but it is completely absent in bulk Eu_2O_3. The broadened spectral lines of the 4-nm sample are consistent with a very disordered cubic phase Eu_2O_3. The spectra of the 18−6-nm particles show that one crystalline phase and one disordered phase are present in the samples. The unanswered question is, what is the physical relationship of these two phases? These two phases could exist as a disordered surface phase surrounding a crystalline interior, or they result from the distribution of particle sizes, with the larger particles producing the sharp-line spectra and the smaller particles producing the broad line. Energy transfer and concentration dependence studies on Eu^{3+}:Y_2O_3 are underway to try and answer this question. The dynamics of the Eu_2O_3 nanocrystals is discussed in section V with the high-resolution spectroscopic results.

In one last nanoparticle example, a polymorph of Y_2SiO_5 containing 5% Eu^{3+} was synthesized as nanosized particles using a sol−gel method.[81] A metal nitrate solution was mixed with an ethanolic solution of $Si(OCH_3)_4$ and heated at 70−80 °C for several hours, followed by annealing at 1100 °C for 3 h. This procedure produced 50-nm particles in the X_1−Y_2SiO_5 polymorph. Low-temperature optical spectra showed four lines in the $^7F_0 \rightarrow {}^5D_0$ excitation spectra. Two lines arise from the two Y^{3+} cation sites in this polymorph. One line is attributed to Eu^{3+} in a secondary phase of Y_2O_3, and

Table 2. Luminescence Lifetimes at 12 K for Monoclinic 0.1% Eu^{3+}:Y_2O_3 (23 nm average diameter)

		site A	site B	site C
$^5D_1$	bulk	71 ± 7 μs	112 ± 6 μs	138 ± 7 μs
	nanocrystal	45 ± 7 μs	117 ± 9 μs	156 ± 8 μs
$^5D_0$	bulk	1.57 ± 0.07 ms	0.78 ± 0.04 ms	0.82 ± 0.04 ms
	nanocrystal	1.75 ± 0.12 ms	1.23 ± 0.09 ms	1.32 ± 0.06 ms

the authors attribute the fourth line to an amorphous phase that is present, on the basis of the broadening of the spectral lines.

IV. Nanostructured Films and Composites

Lasers and amplifiers for optical-fiber communication require hosts with high light throughput, which limits materials to high-quality crystals, glasses, or thin-film waveguides. For thin films to have low losses, the grain size must be sufficiently small to not scatter optical-wavelength light. High-optical-quality films can be prepared by controlling the conditions of typical film preparation methods to maintain nanometer dimensions in the deposited grains. Synthesis methods to grow nanostructured oxide films include spray pyrolysis,[82,83] laser ablation,[84,85] and chemical-vapor-deposition methods.[66,84] The direct deposition of luminescent thin films for display phosphors also has advantages compared to the use of particulate material, such as better adhesion, lower outgassing, and higher resolution.[84,86] FEDs produce a high current density and, therefore, create a higher heat load compared to conventional cathode-ray tubes, and solid films can dissipate the heat better than particles to reduce degradation problems and thermal quenching of the luminescence.[87]

Films of Eu^{3+}:Y_2O_3 achieve luminescence efficiencies that approach commercial phosphors, although many of the as-deposited films require high-temperature annealing.[84−86] Many factors besides the quantum efficiency of the lanthanide determine the overall luminescence efficiency of phosphor films. The luminescence efficiency of Eu^{3+}:Y_2O_3 films prepared by pulsed-laser deposition on diamond-coated Si substrates was approximately a factor of 2 higher than films deposited directly on Si. The increase was attributed to reduced internal reflections due to the rough surface morphology produced by the diamond layer, and the best film (annealed at 700 °C) had 80% of the brightness of Eu^{3+}:Y_2O_3 powder.[88] A spray-pyrolysis deposition method produced luminescent Er^{3+}:Y_2O_3 waveguides with grain size of 20 nm.[83] The as-deposited films emit at 1540 nm and have potential as amplifiers in integrated-optic amplifiers and lasers.

In a unique use of lanthanide-containing films, Langmuir−Blodgett (LB) films containing a europium chelate have been sandwiched between two silver mirrors to form a $\lambda/2$ resonant microcavity.[89] The cavity consisted of 50−52 LB layers, which were each 2.8 nm thick. The remainder of the cavity has the effective optical penetration depth of the light in the silver mirrors (75 nm). The optimum cavity distance was 306.7 nm, which corresponded to one-half of the peak $^5D_0 \rightarrow {}^7F_2$ emission wavelength. With the mirrors present, the photoluminescence intensity increased by a factor of 5 and the emission lifetime decreased from 186 to 104 μs, as expected for resonant enhancement in a cavity.

Films and waveguides can also be prepared by embedding nanoparticles in a polymer composite that matches the refractive index of the particles. Although not yet demonstrated for lanthanide dopants, Barber et al. have demonstrated the principle by achieving relative gain in composites consisting of Cr:forsterite (Cr:Mg_2SiO_4) and Cr:diopside (Cr:$CaMgSi_2O_6$) nanocrystals embedded in index-matching polymer.[9] Net laser amplification is expected with further increases in the quality of the films. This work is significant in that it demonstrates the ability to use nanostructures in optical applications with materials, e.g., diopside, that have not been produced previously as optical-quality crystals.

Research is active and ongoing in glass−ceramic materials[90] and nanocrystal-containing glasses.[91,92] These materials achieve optical properties that are similar to those of lanthanides in crystalline hosts, but with the processibility or compatibility of a glass host. Recent advances have managed to put lanthanide dopants in new hosts or composite environments. Europium and terbium benzoates have been doped into silica glass using a sol−gel technique.[93] In these composites, the benzoate acts as a sensitizer for the lanthanide emitter and increases the luminescence efficiency by factors of 15 and 10 for Eu^{3+} and Tb^{3+}, respectively, when excited at 290 nm. A similar enhancement effect is observed in self-assembled lanthanide-cored dendrimer complexes.[59] Sol−gel techniques have also been used to dope lanthanides in SnO_2 xerogels[94] and in highly porous alumina, which is nanostructured with dimensions of ∼5 nm.[95] Trivalent lanthanides have not previously been substituted into Al_2O_3 due to the size mismatch between the large lanthanide and the small Al^{3+} cation. The characterization of these materials is described in the next section.

V. Dynamic and High-Resolution Spectroscopic Techniques

This section discusses dynamic and high-resolution spectroscopic measurements that are aimed at understanding the size dependence of the physical properties of the insulating host.

The simplest measurements are excited-state lifetime or energy-transfer experiments. High-resolution spectroscopy using hole burning in the inhomogeneously broadened absorption line can measure the homogeneous line width of the transitions, which provides a measure of the phonon dynamics and electron−phonon interaction in the host.[96] The hole burning can arise from a redistribution of population in ground-state hyperfine levels or from a persistent mechanism such as a photochemical change in the local environment of the lanthanide dopant (persistent spectral hole burning, PSHB).

The excited-state lifetimes of the gas-phase condensed nanocrystals changed with particle size, but not in a systematic way. Table 2 shows that most of the excited-state levels of 23-nm 0.1% Eu^{3+}:Y_2O_3 particles have slightly longer lifetimes compared to bulk material.[97]

Table 3. $^5D_0$ Luminescence Decay Times of Eu_2O_3 Nanocrystals at 12 K

average particle diameter	$^5D_0$ decay time (μs)[a]
bulk (>1 μm)	12/61
18 nm	8/36
12 nm	25/250
6 nm	40
4 nm	38

[a] The dual numbers are for a biexponential fit.

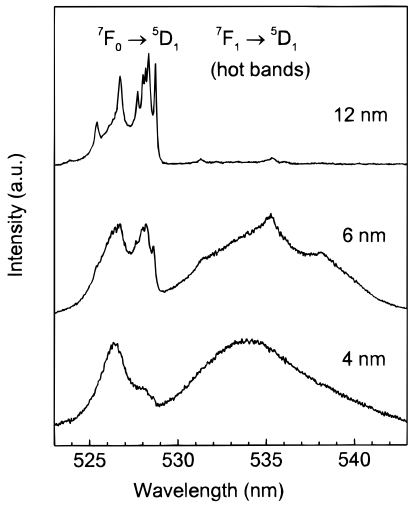

Figure 5. Excitation spectra of nanocrystalline Eu_2O_3 at approximately 12 K showing the $^7F_1 \rightarrow {}^5D_1$ hot-band region. The spectra were recorded with a low-resolution monochromator at 624 nm and a boxcar gate width of 150 μs.

Although the luminescence quantum efficiencies were not measured, there is no shortening of the lifetimes due to increased quenching by surface defects. Table 3 lists the $^5D_0$ lifetimes of the Eu_2O_3 nanocrystals.[30] No clear trend is observed in the $^5D_0$ lifetimes as a function of particle size. An unexplained lengthening of the luminescence decay occurs when the Eu_2O_3 particle diameter decreases from 18 to 12 nm. The luminescence transients of the 6- and 4-nm samples fit well to a single-exponential function. This change from multiexponential to single-exponential decay is attributed to the disappearance of the distribution of cross-relaxation rates, since the small particle diameter essentially eliminates the distribution of distances between Eu ions. This explanation of the single-exponential behavior assumes that there are no ion−ion interactions across the particle interfaces.

Figure 5 shows extended scans of the excitation spectra of the 12-, 6-, and 4-nm Eu_2O_3 particles. A large increase in the intensity of hot bands (see Figure 1) compared to the normal excitation lines occurs as the particle size decreases. There is no line broadening and no observation of hot bands in the luminescence spectra that would indicate that the sample is at an elevated temperature. The increase in hot-band intensity in Figure 5 suggests that the smaller particles have a nonequilibrium storage of population in the $^7F_1$ level and, presumably, also in other low-lying excited states. This result suggests that there is a decrease in the population of optical phonons that facilitates nonradiative relaxation, which is counter to predictions that the density-of-states of high-energy phonons will increase as size-specific resonances become possible in the smaller particle sizes.[34] We have no consistent explanation for this unusual result, but it does suggest that the nonradiative relaxation rates are modified by the size of the nanoparticles.

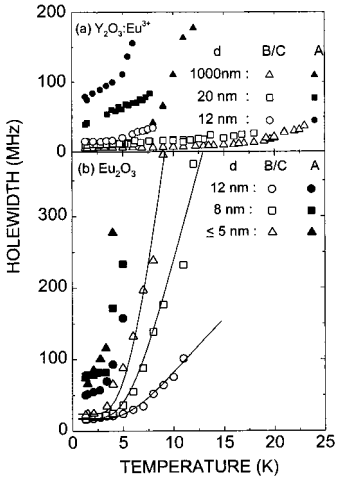

Figure 6. Hole width temperature dependence of the Eu^{3+} $^7F_0 \rightarrow {}^5D_0$ transition as a function of particle size for (a) Eu^{3+}:Y_2O_3 and (b) Eu_2O_3. The solid curves are fits to the data using $A_d e^{-\hbar\omega/kT}$, where A_d is a particle-size-dependent scaling parameter and $\hbar\omega/k = 23$ cm^{-1}.

High-resolution homogeneous line width measurements on Eu_2O_3 and Eu^{3+}:Y_2O_3 nanocrystals show an exponential temperature dependence rather than the more typical linear dependence (see Figure 6).[98] The exponential temperature dependence is attributed to a two-phonon dephasing mechanism, and the exponential term arises due to the size-restricted nature of the phonon density-of-states. Simulations can reproduce the temperature dependence of the line widths, but do not match the particle-size dependence. The data suggest that there is a phonon limit that corresponds to a larger size than the actual physical particle size. One explanation is that the phonon limit arises from propagation of phonons between particles that are in contact. A possible hypothesis that explains this result and the increase in hot-band intensity is that the electron−phonon coupling of the Eu^{3+} ions is different depending on whether they are localized in the bulk or at a surface.

Similar hole-burning studies have been reported on the Eu^{3+}-doped porous γ-Al_2O_3 described above.[99] Two hole-burning mechanisms are observed, one causing transient holes by population redistribution among the hyperfine levels (hole width 100 MHz) and the other a PSHB (hole width ~600 MHz). The PSHB could be associated with a physical rearrangement of the nanostructure. The transient hole line width shows an unusual temperature dependence that can be interpreted as resulting from the size-resonant vibrational modes of the nanocrystal. The nanostructure dimensions eliminate the low-frequency vibrations, providing a cutoff in the phonon density-of-states that depends on particle size. The size-resonant spherical and torsional modes then dominate near the cutoff. Two-phonon Raman scattering due to these modes explains the sharp, nearly exponential rise in the hole line width as a function of temperature above 7 K.

The hole-burning results for both the gas-phase-condensed nanocrystals and the porous γ-Al_2O_3 materi-

als indicate that the hole line widths have an exponential temperature dependence that varies roughly as $1/d^2$. This result is similar to that for semiconducting nanoparticles, assuming the major effect is due to the strength of the electron−phonon interaction. However, the particle-size dependence is inconsistent with a gap in the acoustic phonon spectrum, which the elastic model of a sphere predicts to vary as $1/d$.[100]

VI. Summary and Unanswered Questions

The active research in nanostructured materials has resulted in a wide variety of new synthesis methods to prepare pure and doped insulating nanostructures. Several optical results suggest that these or new materials will have enhanced optical properties for improving actual technological devices. Further refinement is desirable in the synthesis methods to eliminate the need for high-temperature annealing of as-prepared materials, as well as development to possibly scale-up some of the preparation procedures. The defect chemistry in nanostructures has not been addressed, and determining the location, distribution, or segregation of the dopant ions in nanoparticles is still an open area for investigation.

Using nanocrystalline phosphors could be complicated if excitation energy can migrate between phosphor particles. Likewise, the effect of a restricted geometry on the radiative and nonradiative transition strengths for localized emitters has only recently been considered.

Adjusting the nanoparticle size or modifying the surfaces might make it possible to tailor the luminescent properties of a dopant and host. On a speculative note, studying optically active nanostructures could lead to the discovery of new and unexpected optical phenomena due to unpredicted optical confinement or dynamic effects.

Acknowledgment. I thank my co-workers at Virginia Tech, including H. Eilers, B. Bihari, D. Williams, J. Milora, and X. Cheng, and Prof. R. Meltzer for valuable discussions and for sharing his hole-burning results. I also gratefully acknowledge support from a National Science Foundation Career Award (CHE-9502460) and a Research Corporation Cottrell Scholars Award.

References

(1) Fouassier, C. *Curr. Opin. Solid State Mater. Sci.* **1997**, *2*, 231.
(2) Blasse, G. *J. Alloys Compd.* **1995**, *225*, 529.
(3) Blasse, G.; Grabmaier B. C. *Luminescent Materials*; Springer-Verlag: Berlin, 1994.
(4) Ronda, C. R. *J. Lumin.* **1997**, *72−74*, 49.
(5) Hase, T.; Kano, T.; Nakazawa, E.; Yamamoto, H. *Adv. Electronics Electron Phys.* **1990**, *79*, 271.
(6) Blasse, G. *Chem. Mater.* **1989**, *1*, 294.
(7) Blasse, G. *Chem. Mater.* **1994**, *6*, 1465.
(8) Kaminskii, A. A.; Weber, M. J. *Crystalline Lasers: Physical Processes and Operating Schemes*; CRC Press: Boca Raton, FL, 1996.
(9) Barber, D. B.; Pollock, C. R.; Beecroft, L. L.; Ober, C. K. *Optics Lett.* **1997**, *22*, 1247.
(10) Li, Z.; Hahn, H.; Siegel, R. W. *Mater. Lett.* **1988**, *6*, 342.
(11) Suryanarayana, C. *Internat. Mater. Rev.* **1995**, *40*, 41.
(12) Hadjipanayis, G. C.; Siegel, R. W. (Eds.) *Nanophase Materials: Synthesis-Properties-Applications*; NATO ASI Series E Vol. 260; Kluwer: Dordrecht, 1993.
(13) Komarneni, S. *J. Mater. Chem.* **1992**, *2*, 1219.
(14) Andres, R. P.; Averback, R. S.; Brown, W. L.; Brus, L. E.; Goddard, W. A., III; Kaldor, A.; Louie, S. G.; Moscovits, M.; Peercy, P. S.; Riley, S. J.; Siegel, R. W.; Spaepen, F.; Wang, Y. *J. Mater. Res.* **1989**, *4*, 704.
(15) Gleiter, H. *Prog. Mater. Sci.* **1989**, *33*, 223.
(16) Chai, B. H. T.; Payne, S. A. *New Materials for Advanced Solid State Lasers;* MRS Symp. Ser. Vol. 329; Materials Research Society: Pittsburgh, PA, 1994.
(17) Kawano, K.; Arai, K.; Yamada, H.; Hashimoto, N.; Nakata, R. *Solar Energy Mater. Solar Cells* **1997**, *48*, 35.
(18) Bhargava, R. N. *J. Lumin.* **1997**, *72/74*, 46.
(19) Goldburt, E. T.; Kulkarni, B.; Bhargava, R. N.; Taylor, J.; Libera, M. *J. Lumin.* **1997**, *72/74*, 190.
(20) Maestro, P.; Huguenin, D. *J. Alloys Compd.* **1995**, *225*, 520.
(21) Yamamoto, H.; Matsukiyo, H. *J. Lumin.* **1991**, *48&49*, 43−48.
(22) Itoh, T. *Rev. Laser Eng.* **1997**, *25*, 738.
(23) Khairutdinov, R. F. *Colloid J.* **1997**, *59*, 535.
(24) Brus, L. E.; Efros, Al. L.; Itoh, T. (Eds.) "Spectroscopy of isolated and assembled semiconductor nanocrystals", special issue of *J. Lumin.* **1996,** *70*.
(25) Reed, M. A.; Seabaugh A. C. *Adv. Chem. Ser.* **1994**, *240*, 15.
(26) Xiaoya, D.; Geng, L.; Lascola, R.; Wright, J. C. *J. Lumin.* **1997**, *72−74*, 553.
(27) Hoffman, K. R.; DeLapp, K.; Andrews, H.; Sprinkle, P.; Nickels, M.; Norris, B. *J. Lumin.* **1995**, *66−67*, 244.
(28) Ludwig, M. H. *Crit. Rev. Solid State* **1996**, *21*, 265.
(29) Vial, J. C.; Canham, L. T.; Lang, W. (Eds.) "Proceedings of the symposium Light Emission from Porous Silicon" *J. Lumin.* **1993**, *57*.
(30) Tissue, B. M.; Bihari, B. *J. Fluor.* In press.
(31) Bhargava, R. N. *J. Lumin.* **1996**, *70*, 85.
(32) Tao, Y.; Zhao, G.; Ju, X.; Shao, X.; Zhang, W.; Xia, S. *Mater. Lett.* **1996**, *28*, 137.
(33) Bhargava, R. N. Gallagher, D.; Hong, X.; Nurmikko, A. *Phys. Rev. Lett.* **1994**, *72*, 416.
(34) Wolf, D.; Wang, J.; Phillpot, S. R.; Gleiter, H. *Phys. Rev. Lett.* **1995**, *74*, 4686.
(35) Itoh, T.; Furumiya, M. *J. Lumin.* **1991**, *48/49*, 704.
(36) Takagahara, T. *J. Lumin.* **1996**, *70*, 129.
(37) Fomin, V. M.; Gladilin, V. N.; Devreese, J. T.; Pokatilov, E. P.; Balaban, S. N.; Klimin, S. N. *Solid State Commun.* **1998**, *105*, 113.
(38) Warren, W. quoted in *MRS Bull* **1996**, *21* (12), 9.
(39) Schwoebel, P. R.; Brodie, I. *J. Vac. Sci. Technol. B* **1995**, *13*, 1391.
(40) Skandan, G.; Foster, C. M.; Frase, H.; Ali, M. N.; Parker, J. C.; Hahn, H. *Nanostruct. Mater.* **1992**, *1*, 313.
(41) Hahn, H. *Nanostruct. Mater.* **1997**, *9*, 3.
(42) Lee, H. Y.; Riehemann, W.; Mordike, B. L. *Z. Metallk.* **1993**, *84*, 79.
(43) Borsella, E.; Botti, S.; Martelli, S. *Mater. Sci. Forum* **1997**, *235−236*, 261.
(44) Lindackers, D.; Roth, P. *Ber. Bunsen-Ges. Phys. Chem. Chem. Phys.* **1997**, *101*, 1718.
(45) Vogt, G. *Proc. Electrochem. Soc.* **1988**, *5*, 572.
(46) Schmidt, T.; Müller, G.; Spanhel, L. *Chem. Mater.* **1998**, *10*, 65.
(47) Herrig, H.; Hempelmann, R. *Nanostruct. Mater.* **1997**, *9*, 241.
(48) Pileni, M. P. *J. Phys. Chem.* **1993**, *97*, 6961.
(49) Hirai, T.; Sato, H.; Komasawa, I. *Ind. Eng. Chem. Res.* **1993**, *32*, 3014.
(50) Levy, D.; Esquivias, L. *Adv. Mater.* **1995**, *7*, 120.
(51) Lei, Z.; Papaefthymiou, G. C.; Ziolo, R. F.; Ying, J. Y. *Nanostruct. Mater.* **1997**, *9*, 185.
(52) Gutzov, S.; Bredol, M.; Wasgestian, F. *J. Phys. Chem. Solids* **1998**, *59*, 69.
(53) Park, D. G.; Burlitch, J. M. *J. Sol−Gel Sci. Technol.* **1996**, *6*, 235.
(54) Jain, S.; Skamser, D. J.; Kodas, T. T. *Aerosol Sci. Technol.* **1997**, *27*, 575.
(55) Jain, S.; Skamser, D. J.; Kodas, T. T. *Aerosol Sci. Technol.* **1993**, *19*, 411.
(56) Shea, L. E.; McKittrick, J.; Lopez, O. A.; Sluzky, E. *J. Am. Ceram. Soc.* **1996**, *79*, 3257.
(57) Matteazzi, P.; Alcala, M. *Mater. Sci. Eng. A* **1997**, *230*, 161.
(58) Giannelis, E. P. *JOM* **1992** (March), *44*, 28.
(59) Kawa, M.; Fréchet, J. M. *Chem. Mater.* **1998**, *10*, 286.
(60) Eilers, H.; Tissue, B. M. *Mater. Lett.* **1995**, *24*, 261.
(61) Auric, P.; Jarjayes, O. *J. Magnetism Magn. Mater.* **1994**, *138*, 115.
(62) Zhou, H. S.; Honma, I.; Haus, J. W.; Sasabe, H.; Komiyama, H. *J. Lumin.* **1996**, *70*, 21.
(63) Stipkala, J. M.; Castellano, F. N.; Heimer, T. A.; Kelly, C. A.; Livi, K. J. T.; Meyer, G. J. *Chem. Mater.* **1997**, *9*, 2341.
(64) Dieke, G. H. *Spectra and Energy Levels of Rare Earth Ions in Crystals;* Interscience: New York, 1968.
(65) Wright, J. C. *Cryst. Latt. Def. Amorph. Mater.* **1985**, *12*, 505.
(66) West, G. A.; Beeson, K. W. *J. Mater. Res.* **1990**, *5*, 1573.
(67) Tissue, B. M.; Wright, J. C. *J. Lumin.* **1988**, *42*, 173.
(68) Ramponi, A. J.; Wright, J. C. *Phys. Rev.***1987**, *B35*, 2413.
(69) Orozco, E. M.; Mendoza, A. A.; Murrieta, H. S.; Rubio, J. O. *J. Phys. C: Solid. State Phys.* **1987**, *20*, 485.

(70) Dexpert-Ghys, J.; Faucher, M.; Caro, P. *J. Solid State Chem.* **1984**, *54*, 179.
(71) Brundage, R. T.; Yen, W. M. *Phys. Rev.* **1986**, *B34*, 8810.
(72) Warren, G. T.; Holmstrom, S. A.; Yakovlev, N. L.; Yen, W. M.; Dennis, W. M. *J. Lumin.* In press.
(73) Selvin, P. R. *IEEE J. Sel. Top. Quantum Elec.* **1996**, *2*, 1077.
(74) Sheng, K. C.; Korenowski, G. M. *J. Phys. Chem.* **1988**, *92*, 50.
(75) Buijs, M.; Meyerlink, A.; Blasse, G. *J. Lumin.* **1987**, *37*, 9.
(76) Li, Q.; Gao, L.; Yan, D. S. *Nanostruct. Mater.* **1997**, *8*, 825.
(77) Tao, Y.; Zhao, G.; Ju, X.; Shao, X.; Zhang, W.; Xia, S. *Mater. Lett.* **1996**, *28*, 137.
(78) Ye, T.; Zhao, G. W.; Zhang, W. P.; Xia, S. D. *Mater. Res. Bull.* **1997**, *32*, 501.
(79) Bihari, B.; Eilers, H.; Tissue, B. M. *J. Lumin.* **1997**, *75*, 1.
(80) Eilers, H.; Tissue, B. M. *Chem. Phys. Lett.* **1996**, *251*, 74.
(81) Yin, M.; Zhang, W.; Xia, S.; Krupa, J. C. *J. Lumin.* **1996**, *68*, 335.
(82) Gurav, A.; Kodas, T.; Pluym, T.; Xiong, Y. *Aerosol Sci. Technol.* **1993**, *19*, 411.
(83) Hoekstra, T. H.; Hilderink, L. T. H.; Lambeck, P. V.; Popma, Th. J. A. *Opt. Lett.* **1992**, *17*, 1506.
(84) Hirata, G. A.; McKittrick, J.; Avalos-Borja, M.; Siqueiros. J. M.; Devlin, D. *Appl. Surf. Sci.* **1997**, *113/114*, 509.
(85) Jones, S. L.; Kumar, D.; Singh, R. K.; Holloway, P. H. *Appl. Phys. Lett.* **1997**, *71*, 404.
(86) Hirata, G. A.; Lopez, O. A.; Shea, L. E.; Yi, J. Y.; Cheeks, T.; McKittrick, J.; Siqueiros. J. M.; Avalos-Borja, M.; Esparza, A.; Falcony, C. *J. Vac. Sci. Technol. A* **1996**, *14*, 1694.
(87) Itoh, S.; Toki, H.; Kataoka, F.; Tamura, K.; Sato, Y. *Ext. Abs. 3rd Inter. Conf. Sci. Technol. Displ. Phosphors*, Nov. 1997, Huntington Beach, CA.
(88) Cho, K. G.; Kumar, D.; Lee, D. G.; Jones, S. L.; Holloway, P. H.; Singh, R. K. *Appl. Phys. Lett.* **1997**, *71*, 3335.
(89) Zhang, B.; Ma, Y.; Xu, M.; Wu, K.; Huang, C.; Zhao, Y.; Zhuo, D.; Yin, L.; Zhao, X. *Solid. State Commun.* **1997**, *104*, 593.
(90) Tick, P. A.; Borrelli, N. F.; Cornelius, L. K.; Newhouse, M. A. *J. Appl. Phys.* **1995**, *78*, 6367.
(91) Düter, D.; Bauhofer, W. *Appl. Phys. Lett.* **1996**, *69*, 892.
(92) Glass, W.; Toulouse, J.; Tick, P. A. *J. Non-Cryst. Solids* **1997**, *222*, 258.
(93) Qian, G. D.; Wang, M. Q. *J. Phys. Chem. Solids* **1997**, *58*, 375.
(94) Ribeiro, S. J. L.; Pulcinelli, S. H.; Santilli, C. V. *Chem. Phys. Lett.* **1992**, *190*, 64.
(95) Feofilov, S. P.; Kaplyanskii, A. A.; Kutsenko, A. B.; Vasilevskaya, T. N.; Zakharchenya, R. I. *Mater. Sci. Forum* **1997**, *239−241*, 687.
(96) Macfarlane, R. M.; Shelby, R. M. In *Spectroscopy of Solids Containing Rare Earth Ions*; Kaplyanski, A. A., Macfarlane, R. M., Eds.; North-Holland: Amsterdam, 1987; p 51.
(97) Williams, D. K.; Bihari, B.; Tissue, B. M.; McHale, J. M. *J. Phys. Chem. B* **1998**, *102*, 916.
(98) Hong, K. S.; Meltzer, R. S.; Bihari, B.; Williams, D. K.; Tissue, B. M. *J. Lumin.* **1998**, *76−77*, 234.
(99) Feofilov, S. P.; Kaplyanskii, A. A.; Zakharchenya, R. I.; Sun, Y.; Jang, K. W.; Meltzer, R. S. *Phys. Rev.* **1996**, *B54*, R3690.
(100) Tamura, A. *Phys. Rev.* **1995**, *B52*, 2668.

CM9802245